



# Predicting of the Lüders' bands in the processing of TH material in computer environment by means of stochastic modeling

Branimir Barisic<sup>a,\*</sup>, Tomaz Pepelnjak<sup>b</sup>, Miljenko D. Math<sup>c</sup>

<sup>a</sup> Faculty of Engineering, University of Rijeka, Rijeka, Croatia

<sup>b</sup> Faculty of Mechanical Engineering, University of Ljubljana, Ljubljana, Slovenia

<sup>c</sup> Faculty of Mechanical Engineering and Naval Architecture, University of Zargeb, Zargeb, Croatia

## ARTICLE INFO

### Article history:

Received 17 November 2006

Received in revised form

16 August 2007

Accepted 16 September 2007

### Keywords:

Lüders' bands (stretcher strains)

Stochastic modeling

Tinplate processing

## ABSTRACT

The presented work focus on the investigation of the Lüders' bands (hereafter referred to as LB) phenomenon in the computer environment by means of experimental design and stochastic modeling. In this investigation LB emerges in the TH materials processing, i.e. stamping process. In the production of TH materials the problem of Lüders' banding has not been eliminated by the use of a skin pass or roller leveling (because of the tinning process) and is not always overcome by the use of interstitial free steel. Because of that, it is useful to predict LB occurrence before the expensive processing process. On the basis of identified input parameters by means of Box-Vilson's method, an experimental foundation for these investigations has been developed. This basis serves as a fundament for stochastic modeling. By means of stochastic modeling a computer procedure has been developed which will, in the production of practical work, enable the prediction of LB geometrical features ( $l$ : length,  $w$ : width and  $d$ : depth of LB) of predetermined workpieces. The geometrical features of LB originated after varying the input parameters, important in experimental design and stochastic modeling, have been evaluated with instruments for mechanical 3D measurement (Form Talysurf Series 2) as well as for optical 3D digitalization (ZKM 01-250C). The applicability and efficiency of the presented method have been proven by performing the experiment.

© 2007 Elsevier B.V. All rights reserved.

## 1. Introduction

Nonhomogenous yielding and straining of materials is the process of the emergence and subsequent propagation of plastic deformation bands that results in a strain state in which deformation is partly localized and partly retarded or non-existent. These plastic deformation bands have been differently termed: stretcher strains, flow lines, strain figures, stretching figures, plastic flow stress figures, deformation

bands, elongated surface markings, characteristic of no. 5 temper, worms (Barisic, 2005), though most often Lüders' bands or Lüders' deformation and rarely Lüders' lines, named after Lüders (1854) (Lüders, 1860), who discovered them. In 1854 Lüders investigated, and in 1860 he reported that a regular pattern of figures and lines appeared on the surface of rolled steel for spring (Fig. 1) and also on the surface of knives after their manufacture. This phenomenon Lüders observed after the tempering and bending of these products. It is not

\* Corresponding author.

E-mail address: [barisic@riteh.hr](mailto:barisic@riteh.hr) (B. Barisic).

0924-0136/\$ – see front matter © 2007 Elsevier B.V. All rights reserved.

doi:10.1016/j.jmatprotec.2007.09.054

Lüders. über die Aufserung der Elasticität an Stahlstaben &c.

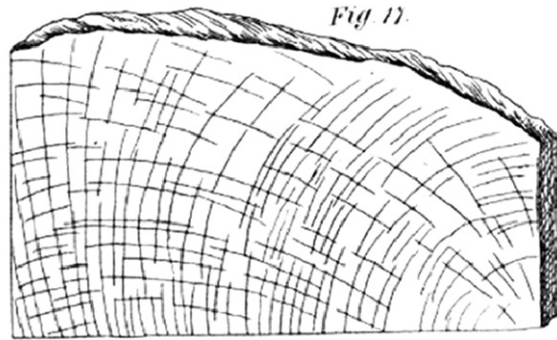


**Fig. 1 – Original figure of lines on the steel for springs from famous Lüders' paper in 1860 (Barisic, 2005).**

widely known that the first discoverer of this phenomenon was A. Piobert in 1842 and because of that some scientists call this type of deformation Piobert–Lüders' bands (Piobert et al., 1842). Also, for the same bands there exist the terms Chernov's bands (Čaušević, 1979) and Hartmann's bands (Hartmann, 1896) according to the scientists who observed them, nonetheless both of them later than Lüders. Also, it can be found in literature that some authors will confuse Lüders' bands with slip lines. The slip lines are intersections of slip surfaces with the other surfaces of a crystal. A lot of crystals cooperate to create a Lüders' band where each of them slips on its slip surface.

Numerous investigations have been performed on the LB phenomenon but despite all of the research effort put into this phenomenon over the years, the basic mechanism underlying the LB phenomenon is still not well understood. A similar situation surrounds the discoverer of LB, in that the notion of Lüders' bands is well-known world wide, but nobody has any further information about him, not even his first name (except for the first letter as an initial).

Investigations regarding the dislocations theory and microstructural parameters (grain size, precipitate concentration, solutes, impurity atoms, etc.) have been shown to influence the occurrence and propagation of LB (Low and Gensamer, 1944; Cottrell, 1948; Gilman, 1959; Ananthan and Hall, 1987; Wen and Morris, 2004). Many studies have dealt with the macrostructural parameters and testing variables (thermal variables, strain rate, investigation devices, specimen geometry, etc.) (Ananthan and Hall, 1987, 1991; Sylwestrowicz and Hall, 1951; Lomer, 1952; Conrad, 1962). In addition, nowadays modern advanced methods use radiation, magnetic flux sensors, digital image correlation (speckle image processing), infrared image processing, thermal activation, magnetic Barkhausen noise and magnetic flux leakage signals, and laser scanning extensometry (Rowcliffe et al., 2000; Kuroda et al., 2001; Wattrisse et al., 2001; Louche and Chrysochoos, 2000; Jones and Feng, 2001; Dhar et al., 2002; Casarotto et al., 2003) for investigation into this phenomenon. The numerous mathematical formulations for LB propagation in tensile testing have been derived using the Prandtl-Reuss stress–strain relations for plastic flow, equations of motion, the incompressibility condition, the quadratic yield condition, modified

Prandtl-Reuss equations, the von Mises stress–strain relations, dynamical conditions, the Hall-Patch law, variations of the dislocation glide velocity, the Fisher Kolmogorov equation, etc. (Thomas, 1954, 1958; Hähner, 1993). Better knowledge of LB, supported by numerical computer simulations, was of help in the prediction of their propagation. A suitable approach in the finite element method is the tangent modulus method that is based on the linearity of the incremental laws of plasticity (Iricibar et al., 1977). A typical stress–strain curve, composed of two straight lines, roughly describes the physical basis of the Lüders' behavior. This local behavior can be introduced in a finite element code to simulate the structural part of the Lüders' phenomenon. Results have shown that some LB can be generated either with a geometrically regular mesh or with a more random mesh (Tsukahara and Jung, 1998). A viscoplastic constitutive model, which can accurately describe the yield point phenomenon and the corresponding cyclic plasticity behavior, has been proposed by Yoshida (Sun et al., 2000) and it is based on the dislocation multiplication theory (Gilman, 1959). This model is founded upon the relationship between the shear plastic strain rate and the dislocation velocity as a function of the applied stress state. Through the use of a non-monotonic uniaxial model for the calibrating of the finitely deforming  $J_2$  flow rule with isotropic hardening, in which trilinear stress–strain approximation is fitted to obey material response (consistent with the tensile test), Lüders' behavior can be obtained (Corona et al., 2002).

The majority of papers regarding LB have analyzed plane-strain conditions by tensile test, however LB as appearing in production and materials processing have rarely been discussed, a matter that is addressed in this paper. According to the knowledge of this paper authors, no one has done this type of analysis regarding LB formation and propagation. The finite element analysis with ABAQUS program in order to analyse the phenomenon of the stretcher strains on an industrial case study can be introduced (Pepelnjak and Barisic, 2007). This research will use stochastic (Barisic et al., 2004; Gantar and Kuzman, 2005) or empirical–statistical models. The development of the stochastic model will be based on statistical processing of experimental data from the previously determined experimental design. For the purpose of deriving an algorithm of stochastic model development a computer program will be configured to the analyzed process. Therefore, the entire process of stochastic model forming will be performed with the help of specially arranged computer procedures such that for the appropriate format, the input parameters are entered, and then at the output the decoded stochastic models that describe the Lüders' bands' geometrical features are directly obtained.

## 2. Material

Tinplate is low carbon steel between 0.13 and 0.50 mm thick coated with between 5.6 and 22.4 g tin/m<sup>2</sup> (EN, 2001). As an eco-friendly packaging material with 100% recyclability it possesses excellent drawability combined with good strength and due to the unique properties of tin it has a good solderability and corrosion resistance and an attractive appearance. Because of that in the canmaking industry, i.e. in the stamp-

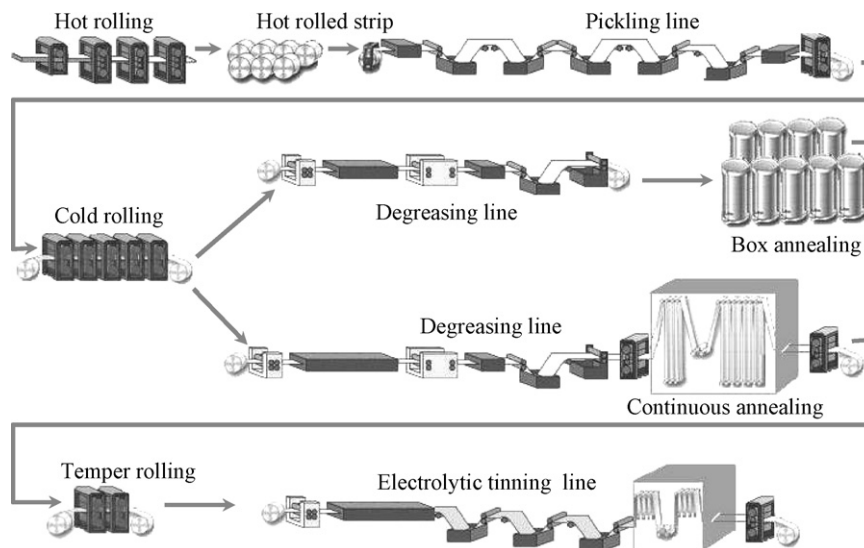


Fig. 2 – Outline of tinplate production.

ing processes of lids, ring cans, ends, etc., its uses is widely acceptable.

Tinplate type TH at about 0.1–0.12% carbon would be our area of interest. At room temperature and under equilibrium conditions, this steel will consist of two phases:  $\alpha$ -iron, termed ferrite, having a body-centered cubic (BCC) structure, and pearlite, a physical mixture consisting of iron carbide ( $\text{Fe}_3\text{C}$ ) and ferrite. Our TH 0.08% carbon steel consists of 85–87.5% of ferrite and 12.5–15% of pearlite.

### 3. Cause of Lüders' bands formation

In the production of tinplate (Fig. 2) this material hardens after cold rolling due to the strain hardening generated by plastic deformation. Annealing is therefore carried out to soften the material and to remove the hardening. For this purpose, there are two processes of annealing (batch and continuous annealing, Fig. 2) and the process that will be used depends on which one will best achieve the required material properties. Batch annealed tinplates due to their high aging resistance (achieved due to the precipitation of nitrogen as  $\text{AlN}$  and carbon in the form of stable carbides and without dispersion and precipitate hardening, by means of the low cooling rates inherent to the batch or box annealing process) are better in subsequent forming processes. Tinplate following the batch annealing process is designated as tinplate type TS. Continuous annealed tinplates due to their time and cost savings

have become more common. Also, the more homogeneous conditions in this process reduce variation in the mechanical properties of continuous annealed tinplates. However, they exhibit low aging resistance, because considerable amounts of carbon and nitrogen atoms remain in the interstitial solid solution in ferrite after the continuous annealing cycle, which leads to non-uniform straining. Tinplate after the continuous annealing process is designated as tinplate type TH.

#### 3.1. Aging

Cold rolled and annealed low carbon steel strip is important to avoid aging, as this causes discontinuous yielding, non-uniform straining and localized thinning during the subsequent stamping process followed by LB propagation. This appearance is accompanied with the yield point phenomenon on the stress-strain curve. Because this consistent straining results in the formation of LB with an unacceptable ripple in the surface finish, it could be concluded that aging could be commercially important because during tinplate stamping the occurrence of LB gives a wrinkled finish as a result of the aging processes. The aging process is a transformation in which the features of a material change over time in the transfer from its nonequilibrium to equilibrium state. Aging process can be artificial or thermal aging and natural or strain aging. The strain aging occurs at ambient temperatures and thermal aging at raised temperatures (from  $50^\circ\text{C}$  and upwards). The nonequilibrium state in the structure of steel can be provoked

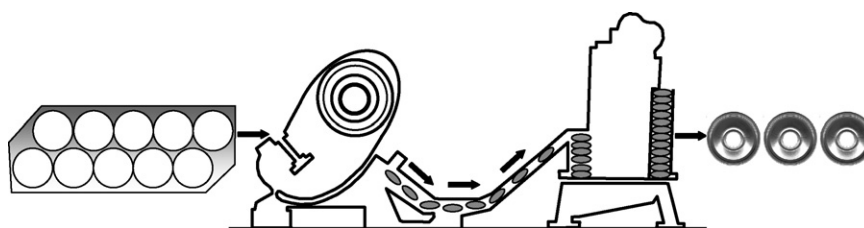


Fig. 3 – Lids (ends) stamping process.

by determined technological parameters in manufacturing, i.e. in heat treatment–thermal aging, and it can also be provoked during subsequent cold working (in stamping)–strain aging. Both types of aging are presented in the manufacturing of tinsplate products. Thermal aging (artificial) is presented in the process of continuous annealing and again in the process of tinning (Fig. 2). Strain aging is presented in the process of subsequent stamping (Fig. 3).

Aging and its consequences in the form of LB are associated with the pinning of dislocations. The pinning of dislocations could be caused by many separate microstructural features, which obstruct the movement of dislocations. Some of microstructural features that obstruct free dislocation movement are: precipitates, grain boundaries, fine grain size, other dislocations, impurity atoms, other atoms, particles, etc. When the dislocations in tinsplate type TH are pinned, the pinning forces are so strong that the dislocations cannot break away unless the local stress is very high. For the movement of the pinned dislocations a high stress (upper yield strength at the stress–strain curve) is required. After unpinning, the stress decreases until the mobility of the dislocation is interrupted (different microstructural obstacles). Again a stress increase is necessary to unpin dislocations within the adjacent grain. As plastic deformation is not uniform but rather takes place only locally due to the movement of mobile dislocations, the characteristic LB appear.

### 3.2. Thermal aging

Thermal aging refers to a process in which the properties of a material change because of accelerated cooling from the annealing temperature. Accelerated cooling in the tinsplate continuous annealing process of type TH will result in a supersaturated solution of carbon and nitrogen in ferrite, thus avoiding the precipitation of carbon and nitrogen in the form of carbides and nitrides, which means a dangerous supersaturation. Interstitial carbon and nitrogen atoms emerge in this way, migrating to dislocations and pinning them, thus increasing strength, reducing ductility and the appearance of LB. Also, the cooling time in this process is too short for coalescence and grain growth and the ferrite grain size is inevitably small, which is ideal for the prevention of dislocation mobility. With aging at temperatures that permit the solutes to diffuse, dislocations are pinned and become immobile because the dislocation is moved away from the segregated solute. It is possible to prevent aging and LB through the application of a small cold rolling reduction (called temper rolling or skin pass, Fig. 2) after continuous annealing. In this way the greater density of forest dislocations emerges which will enable a homogenous plastic straining to occur. However, after the tinning process (Fig. 2) the thermal aging and Lüders' bands will reappear immediately.

### 3.3. Strain aging

Strain aging refers to a process in which the dislocation density is increased by plastic straining during cold metal formation and after which the material is held at room temperature long enough for nitrogen and carbon atoms to diffuse to the cores of the dislocations and immobilize them. In tin-

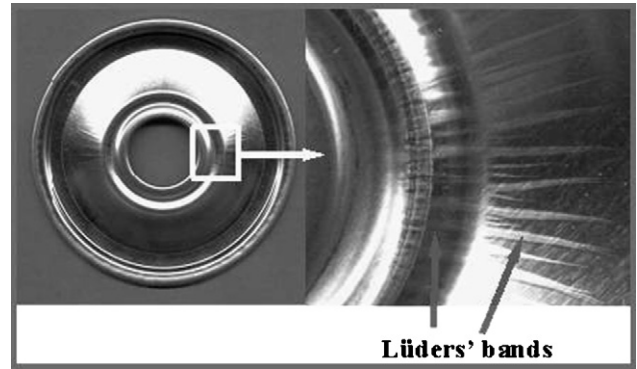


**Fig. 4 – Lüders' bands emerging after lids (ends) stamping process.**

plate type TH the strain aging will appear if after process of temper rolling material is held at room temperatures for about 1 month and after that is processed. When plastic deformation (e.g. the stamping of container lids) begins it does so only in some particular places of the workpiece where there are localized stress concentrations that are able to generate or activate dislocation sources, which lead to the emergence of LB. When the dislocation sources are generated they create new dislocation lines and the number of mobile dislocations increases rapidly. The interactions between interstitial solute elements and dislocations in BCC structure at room temperatures are very strong. Nitrogen diffuses faster than carbon does at room temperature and it has a higher solubility in ferrite at this temperature.

If Lüders' elongation appears in the stress–strain curve, it does not mean that LB will appear during the forming of different workpieces. In the stamping of ends (lids, rings, etc.) from tinsplate, type TH will appear (Fig. 4) but in the deep drawing or ironing of cans, rolling of can bodies will not. During the forming process, the material undergoes different stress–strain conditions and LB will appear only in the stress–strain area corresponding to the pinning of dislocations, i.e. yield point elongation in the stress–strain curve (this deformation state match the process of ends stamping). In the area out of yield point elongation in the stress–strain curve there is no pinning of dislocations and LB will not appear (this deformation state match the process of deep drawing or ironing).

## 4. Experimental design

In the development of the experimental–computational technique, economic and technological demands for the method of experiment design in view of reduction of the number, duration and expensive of experimental research, and in addition to obtaining reliable anticipations of complex research, require the use of experimental design methods in the complex research process. The multifactor experiment design method will be applied in the area of the experimental design of this research. Specifically, the multifactor central compositional rotatable plan is involved. These experimental designs have a minimal number of experimental points positioned according to a defined algorithm—multifactor design in exper-

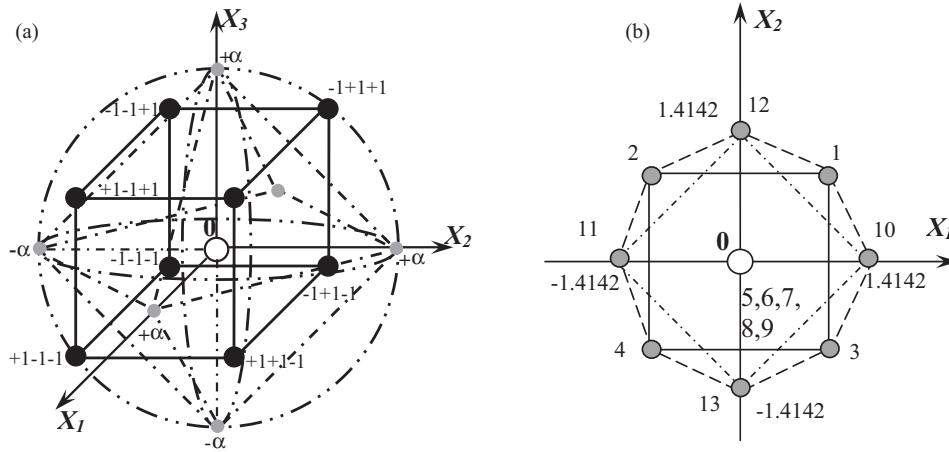


Fig. 5 – Graphic presentation of central composition design (a) and rotatable design (b).

imental hyperspace. This considerably reduces the cost and duration of expensive experimental research. These designs also provide a maximum of information on process model effects, which is achieved by a special plan of point arrangement in the experimental hyperspace based on optimality criterion. All factors are altered simultaneously, therefore every model parameter is determined on the basis of all  $N$  experimental results, the consequence of which is that the dispersion  $\sigma^2(b_i)$  of any  $b_i$  model coefficient is  $N$  times smaller than experimental error. The dispersion  $\sigma^2(b_i)$  of model parameters is minimal, which leads towards greater precision and reliability of the required function  $y$  of the process description. This active experimental design is often applied in modeling and adaptive managing of processes with several variables. The schematic outline of the central composition design is presented in Fig. 5a, and the schematic outline of the rotatable design involved in this paper is presented in Fig. 5b. These experimental designs have an elementary part  $2^k$  ( $k$ -number of varying variables in the process), a symmetric set points  $n_\alpha$  around the center of design (their number is  $2k$ ), and repetition points  $n_0$  at the center of the design. The matrix of the experimental design with varying variables, tool velocity and friction coefficient ( $v, \mu$ ), is formed on the

basis of rotatable design (Table 1). This matrix is used for six different grain size diameters  $d_g$  ( $d_{g1} = 4.5 \mu\text{m}$ ,  $d_{g2} = 5.15 \mu\text{m}$ ,  $d_{g3} = 5.6 \mu\text{m}$ ,  $d_{g4} = 6.7 \mu\text{m}$ ,  $d_{g5} = 7.9 \mu\text{m}$ ,  $d_{g6} = 8.65 \mu\text{m}$ ) regarding the modeling of length, width, and the depth of LB. The friction coefficient values and their influence on material surface have been determined experimentally by means of tribometer Tritop. Also, tool velocity has been determined experimentally by means of special equipment for measuring of tool velocity.

### 5. Experimental measurement

After the formation of experiment design, experimental research has been conducted, as well as providing the definition of the geometrical features needed for the formation of stochastic models. Methods of mechanical measurement of workpieces for the establishment of geometrical features using 3D coordinate measuring systems, Form Talysurf Series 2 (Taylor-Hobson Ltd., Leicester, Great Britain) are applied to simultaneously define the dimensions, form and texture of the surface. Similar type of device was used by Tay et al. (2002) at a study of surface roughness parameters of the flank wear surface. Basic data for this measuring device are: transversal

Table 1 – Rotatable experimental design matrix along with the measuring results of LB geometry regarding  $l$ : length,  $w$ : width, and  $d$ : the depth of LB

| Number of experiments | Coded values |        |        |          |         |         | Physical values |                  | Geometry of LB |          |          |
|-----------------------|--------------|--------|--------|----------|---------|---------|-----------------|------------------|----------------|----------|----------|
|                       | $X_0$        | $X_1$  | $X_2$  | $X_{12}$ | $X_1^2$ | $X_2^2$ | $\mu$           | $v, \text{mm/s}$ | $w$            | $l$      | $d$      |
| 1.                    | 1            | +1     | +1     | 1        | 1       | 1       | 0.15            | 2.7              | $w_1$          | $l_1$    | $d_1$    |
| 2.                    | 1            | -1     | +1     | 1        | 1       | 1       | 0.05            | 2.7              | $w_2$          | $l_2$    | $d_2$    |
| 3.                    | 1            | +1     | -1     | -1       | 1       | 1       | 0.15            | 0.5              | $w_3$          | $l_3$    | $d_3$    |
| 4.                    | 1            | -1     | -1     | -1       | 1       | 1       | 0.05            | 0.5              | $w_4$          | $l_4$    | $d_4$    |
| 5.                    | 1            | 0      | 0      | 0        | 0       | 0       | 0.1             | 1.6              | $w_5$          | $l_5$    | $d_5$    |
| 6.                    | 1            | 0      | 0      | 0        | 0       | 0       | 0.1             | 1.6              | $w_6$          | $l_6$    | $d_6$    |
| 7.                    | 1            | 0      | 0      | 0        | 0       | 0       | 0.1             | 1.6              | $w_7$          | $l_7$    | $d_7$    |
| 8.                    | 1            | 0      | 0      | 0        | 0       | 0       | 0.1             | 1.6              | $w_8$          | $l_8$    | $d_8$    |
| 9.                    | 1            | 0      | 0      | 0        | 0       | 0       | 0.1             | 1.6              | $w_9$          | $l_9$    | $d_9$    |
| 10.                   | 1            | 1.414  | 0      | 0        | 2       | 0       | 0.171           | 1.6              | $w_{10}$       | $l_{10}$ | $d_{10}$ |
| 11.                   | 1            | -1.414 | 0      | 0        | 2       | 0       | 0.029           | 1.6              | $w_{11}$       | $l_{11}$ | $d_{11}$ |
| 12.                   | 1            | 0      | 1.414  | 0        | 0       | 2       | 0.1             | 3.2              | $w_{12}$       | $l_{12}$ | $d_{12}$ |
| 13.                   | 1            | 0      | -1.414 | 0        | 0       | 2       | 0.1             | 0.045            | $w_{13}$       | $l_{13}$ | $d_{13}$ |

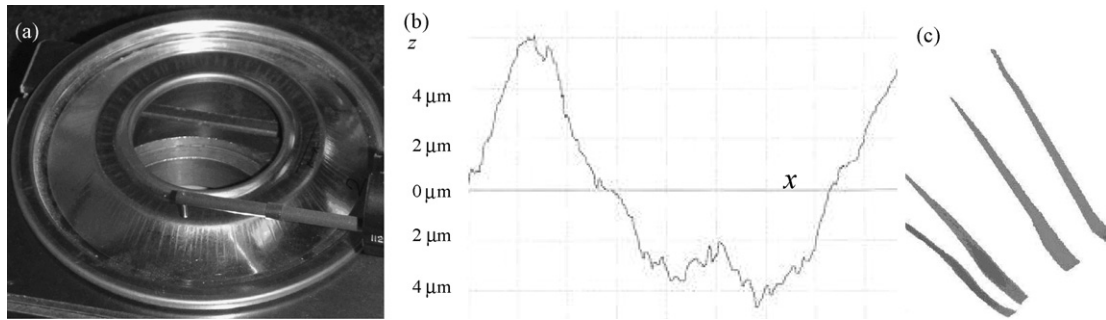


**Fig. 6 – The measurement of Lüders’ bands geometrical features (a), the writing out of profile in x–z direction (b) and 3D surface topography picture (c).**

precision 300 nm, longitudinal precision 1 nm, measuring distance 5.2 cm and maximal angle 12°. This device uses powerful software to combine data generated by longitudinal movement of the stylus with data collected from the linear scale and reading head in the transversal traverse unit. The result is a grid array of a cloud of data points.

Measurement was conducted by means of a method in which the first profile surface was taken from one direction. Afterwards, the measured coordinates (x and z) were input into the program and the profile surface was taken from the other direction. In this way, the measured coordinates (y and z) are obtained and a 3D surface topography is composed. Using the methods mentioned, the measurement of the LB geometrical features was performed. Samples are digitalized with the purpose of establishing geometrical features, and checking is executed using the optical measuring system ZKM 01-250C (Carl Zeiss, Jena, Germany). The measurement of the LB geometrical features, the writing out of the profile in x–z direction, and a 3D surface topography are presented in Fig. 6.

### 6. Stochastic modeling and computer calculation procedure

Since processing processes, like other technological processes, are of a stochastic character, this research uses the method of stochastic modeling. This research will deal with stochastic models of the empirical–statistical type belonging to the class of elliptical models and as such do not contain the component of time in their function response. The component of time in the discontinuous interval is established and indirectly contained through the mechanism of interactions and unfamiliar regularities during the process in the form of insignificant

noise (Nelson, 1995). The course of discontinuous time interval (e.g. the measuring of results from sharpening to the sharpening of the tool in the process of stamping) does not show its influence on the output process parameters (such as depth, width or length of strains in nonhomogeneous yielding, deformation force of the process, strain energy, etc.), contrary to the prominent influence of significant input parameter variation. The probability theory along with the theory of stochastic processes is the starting point for the study and analysis of stochastic processes of this type. This research will use stochastic or empirical–statistical models which start from the function of the process state ( $\bar{y}$ ), that is, from the vector of the process features obtained by measuring as the process result. The development of the stochastic model will be based on the statistical processing of experimental data from the previously determined experimental plan. After the choice of influential parameters for model formation in accordance with the experimental matrix design, the coding of influential parameters for each geometric and material toll (different  $d_g$ ) are performed. In Table 2 the coded and physical values of influential parameters prepared for the stochastic modeling have been shown. Development of the computer program for the analyzed process has been built to the stochastic model algorithm. Therefore, the entire process of stochastic model forming will be performed with the help of specially arranged computer procedures, so that for the appropriate format the input parameters are entered, and then at the output decoded stochastic models are directly obtained. It means that for adequate format (e.g.  $d_{g1}$ , lids 1) the input parameters ( $l$ ,  $w$ , and  $d$  of LB as measured values) have been entered and the output coded stochastic model has been obtained. In Fig. 7 the algorithm of stochastic model development and its computer program have been presented. On the basis of the presented

**Table 2 – Coded and physical values of influential parameters prepared for the stochastic modeling**

| Variables domain       | Coded values   |            |           |           |                 |
|------------------------|--|------------|-----------|-----------|-----------------|
|                        | $X_1 (-1.4142)$  | $X_2 (-1)$ | $X_3 (0)$ | $X_4 (1)$ | $X_5 (-1.4142)$ |
| Physical values        |  |            |           |           |                 |
| $x_1 = \mu$ (mm/s)     | 0.029  | 0.05       | 0.1       | 0.15      | 0.171           |
| $x_2 = v$ (mm/s)       | 0.045  | 0.5        | 1.6       | 2.7       | 3.2             |
| Average grain diameter | $d_{g1} = 4.53; d_{g2} = 5.15; d_{g3} = 5.6; d_{g4} = 6.7; d_{g5} = 7.9; d_{g6} = 8.65; \dots$ |            |           |           |                 |
| Workpiece geometry     | Lid 1, lid 2, ..., ring 1, ring 2, ...   |            |           |           |                 |

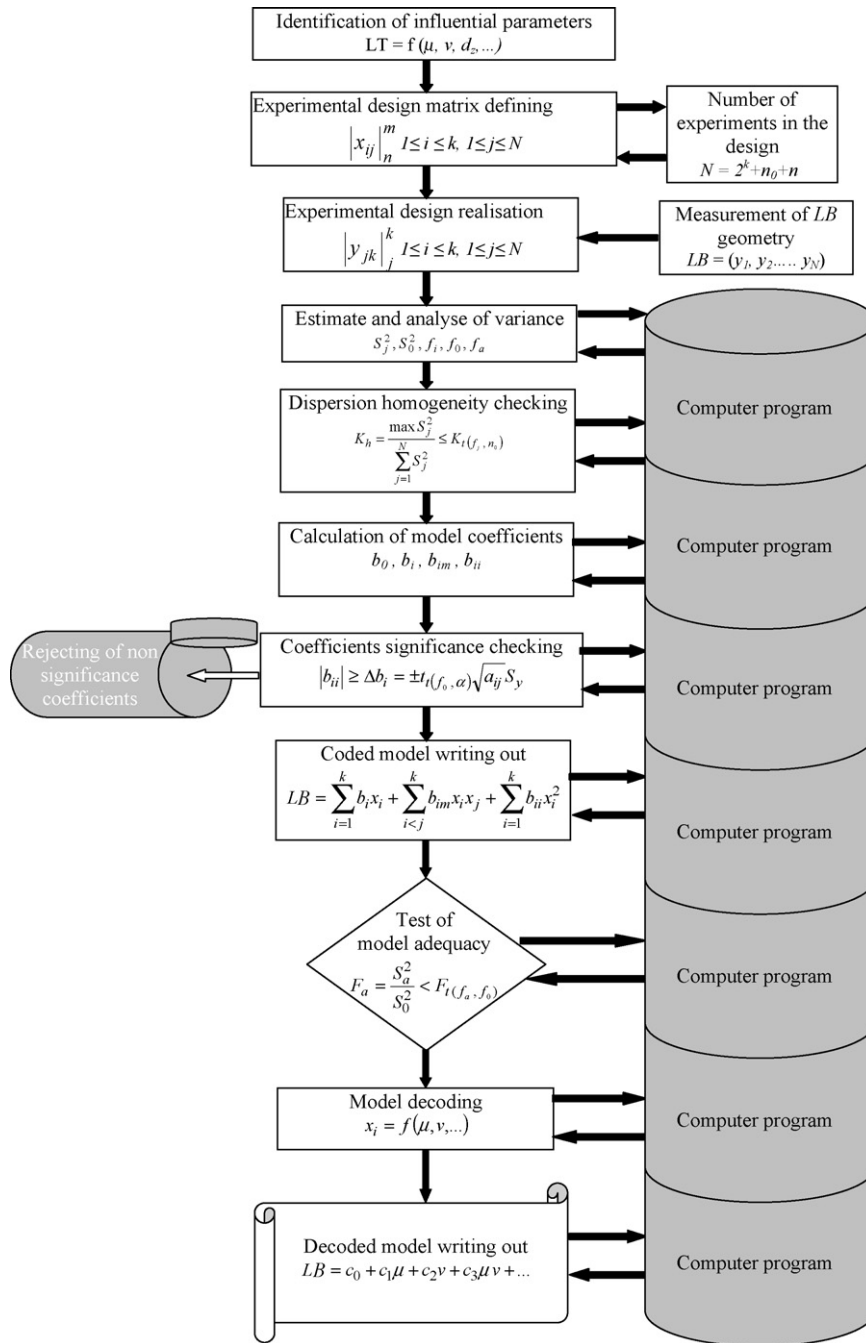


Fig. 7 – The algorithm of stochastic model development and its computer program.

algorithm, a program solution in Mathematica v.6 has been developed. The sequence of calculations and formulae used in the computer program has been shown in the following subchapters.

6.1. Model introducing

For the modeling of the output parameters of the geometry of LB (l, w, d), the second order model has been introduced:

$$Y = b_0 + b_1x_1 + b_2x_2 + b_3x_3 + b_{12}x_1x_2 + b_{11}x_1^2 + b_{22}x_2^2 \quad (1)$$

In this way the form of polynomial approximates the determined problem and the solving comes down to the calculation of coefficients  $b_i$ . Coded and physical values of processes along with their interactions are presented in Table 1. Examination of the dispersion homogeneity of experimental results has been performed according to equation (Cochran's criterion for the level of reliability  $P = 0.95$ ):

$$K_h = \frac{\max S_j^2}{\sum_{j=1}^N S_j^2} K_{t(f_j, n_0)} \quad (2)$$

where  $\max S_j^2$  is the maximal variance at the center of design,  $K_t$  is the value according to Cochran's criterion for degrees of freedom  $f_j$  and  $N$ ,  $K_{t(4,5)}$  for  $\alpha=0.05=0.544$ ,  $f_j$  is the degree of freedom,  $f_j=n_j-1$ ,  $n_0$  is the repetition points at the center of design,  $\sum_{j=5}^9 S_j^2 = S_0^2$  is the variance of central points of rotatable design.

If the dispersion homogeneity criterion is satisfied, then calculation of mathematical model coefficients can be conducted.

6.2. Calculation of mathematical model coefficients

Calculation of mathematical model coefficients has been performed according to following formulae:

$$b_0 = a_1 \sum_{j=1}^N Y_j + a_2 \sum_{i=1}^k \sum_{j=1}^N X_{ij}^2 Y_j, \tag{3}$$

$$b_i = a_3 \sum_{j=1}^N X_{ij} Y_j, \tag{4}$$

$$b_{im} = a_4 \sum_{j=1}^N X_{ij} X_{mj} Y_j, \tag{5}$$

$$b_{ii} = a_5 \sum_{j=1}^N X_{ij}^2 Y_j + a_6 \sum_{i=1}^k \sum_{j=1}^N X_{ij}^2 Y_j + a_7 \sum_{j=1}^N Y_j, \quad i = 1, 2, 3. \tag{6}$$

where  $a_i$  is the table values for  $k=2$ ,  $n_0=5$  and  $N=13$ ,  $a_1=0.2$ ;  $a_2=-0.1$ ;  $a_3=0.125$ ;  $a_4=0.25$ ;  $a_5=0.125$ ;  $a_6=0.01875$ ;  $a_7=-0.1$ ;  $X_{ij}$  and  $Y_j$  are the coded values.

After the calculation of mathematical model coefficients the checking of model significance can be performed.

6.3. Checking of significance by means of Student's t-criterion

Checking of model significance by means of t-criterion has been determined according to expression:

$$|b_{ii}| \geq \Delta b_i = \pm t_{t(f_0, \alpha)} \sqrt{a_{ij}} S_y, \tag{7}$$

i.e., for each coefficient, which means

$$\begin{aligned} |b_0| &\geq \Delta b_0 = \pm t_{t(f_0, \alpha)} \sqrt{a_{11}} S_y, \\ |b_i| &\geq \Delta b_i = \pm t_{t(f_0, \alpha)} \sqrt{a_{12}} S_y, \quad |b_{im}| \geq \Delta b_{im} = \pm t_{t(f_0, \alpha)} \sqrt{a_{13}} S_y, \\ |b_{ii}| &\geq \Delta b_{ii} = \pm t_{t(f_0, \alpha)} \sqrt{a_{14}} S_y \end{aligned} \tag{8}$$

where  $t_{t(f_0, \alpha)} = t_{t(4, 0.05)} = 2.13$  (table values for Student's t-criterion),  $a_{ij}$  is the elements of correlation matrix,  $a_{11}=0.2$ ;  $a_{12}=0.125$ ;  $a_{13}=0.25$ ;  $a_{14}=0.14375$ .

After the checking of model coefficients, the significance of the coded stochastic model has been obtained and this step is needed to estimate its adequacy. The checking of model adequacy has been performed by means of Fisher's F-criterion.

6.4. Checking of adequacy by means of Fisher's F-criterion

Checking of model adequacy by means of the F-criterion has been determined according to the condition:

$$F_a = \frac{S_a^2}{S_0^2} < F_{t(f_a, f_0)} = F_{t(3, 4)} = 6.59 \text{ za } \alpha = 0.05. \tag{9}$$

Adequacy dispersion  $S_a^2$  has been determined according to the expression:

$$S_a^2 = \frac{\sum_{j=1}^N (y_j^E - y_j^R)^2 - \sum_{j=1}^{n_n} (y_{0j} - \bar{y}_0)^2}{f_a}, \tag{10}$$

where  $f_a$  is the degree freedom number for adequacy dispersion,  $f_a = N - 0.5(k + 1)(k + 2) - (n_0 - 1)$ , i.e.  $f_a = 13 - 0.5(3 \cdot 4) - (5 - 1) = 3$  for this experimental model,  $\sum_{j=1}^{n_n} (y_{0j} - \bar{y}_0)^2$  is the quadratic expression of the difference in experimental and calculated values of the response function in zero points,  $(y_j^E - y_j^R)^2$  is the quadratic expression of the difference in experimental and calculated values of response function in all points.

If the dissipation of experimental results in the central point of design is too large or too small, and on the basis of the F-criterion it is not possible make a decision, thus as a complementary criterion of model adequacy the coefficient of multiregression R has to be introduced. This coefficient for experimental design has the form:

$$R = \sqrt{1 - \frac{\sum_{j=1}^N (y_j^E - y_j^R)^2}{\sum_{j=1}^N (y_j^E - \bar{y}^E)^2}}, \tag{11}$$

where  $\bar{y}^E = \frac{\sum_{j=1}^N y_j^E}{N}$  is the arithmetic mean of all experimental results.

Following model decoding, i.e. coded values, the introduction of stochastic models in their physical forms is obtained. All obtained stochastic models are coded according to the expression:

$$X_1 = \frac{\mu - 0.1}{0.05}, \tag{12}$$

$$X_2 = \frac{v - 1.6}{1.1}. \tag{13}$$

7. Results analysis

If the results of length  $l$  (for each grain: rolling direction, direction of 45° to rolling, direction of 90° to rolling), width  $w$  (for each grain: rolling direction, direction of 45° to rolling, direction of 90° to rolling) and depth  $d$  of LB has been taken, then there are 258 stochastic models only for lids 1 (Ø83.5/Ø24-*Fig. 2*) in measurement of  $b$  and  $w$  to 1 mm of the total length of bands (from the top of the workpiece). The results for other distances and workpieces (lid 1, lid 2, ..., ring 1, ring 2, ... in computer simulation) are not presented due to page space limitation. Obtained computer

**Table 3 – Measured results of LB geometrical features (6 mm from the top of workpiece for *l* and *w* and at the distance of 8.1 mm from the top of workpiece for *d*)**

| $d_g = 5.6 \mu\text{m}$ | $v$ [mm/s] $\mu$ |       | Width/length<br>LB [mm]<br>0° | Width/length<br>LB [mm]<br>45° | Width/length<br>LB [mm]<br>90° | Depth [ $\mu\text{m}$ ] at<br>8.1 mm |      |
|-------------------------|------------------|-------|-------------------------------|--------------------------------|--------------------------------|--------------------------------------|------|
|                         |                  | 2.7   | 0.15                          | 0.55 / 9.7                     | 0.61 / 10                      | 0.66 / 10.2                          | 8.4  |
|                         | 2.7              | 0.05  | 0.54 / 9.2                    | 0.61 / 9.6                     | 0.65 / 9.6                     | 8.3                                  |      |
|                         | 0.5              | 0.15  | 0.68 / 9.7                    | 0.79 / 10                      | 0.83 / 10.2                    | 2.8                                  |      |
|                         | 0.5              | 0.05  | 0.67 / 9.2                    | 0.77 / 9.6                     | 0.81 / 9.6                     | 2.6                                  |      |
|                         | 1.6              | 0.1   | 0.60 / 9.4                    | 0.69 / 9.8                     | 0.73 / 9.9                     | 5.6                                  |      |
|                         | 1.6              | 0.17  | 0.61 / 9.8                    | 0.70 / 10.1                    | 0.74 / 10.3                    | 5.7                                  |      |
|                         | 1.6              | 0.03  | 0.59 / 9                      | 0.68 / 9.5                     | 0.72 / 9.5                     | 5.5                                  |      |
|                         | 3.2              | 0.1   | 0.53 / 9.5                    | 0.58 / 9.8                     | 0.62 / 9.9                     | 9.5                                  |      |
|                         | 0.045            | 0.1   | 0.74 / 9.5                    | 0.87 / 9.8                     | 0.9 / 9.9                      | 1.5                                  |      |
| $d_g = 6.7 \mu\text{m}$ | $v$ [mm/s] $\mu$ |       | Width/length<br>LB [mm]<br>0° | Width/length<br>LB [mm]<br>45° | Width/length<br>LB [mm]<br>90° | Depth [ $\mu\text{m}$ ] at<br>8.1 mm |      |
|                         |                  | 2.7   | 0.15                          | 0.57 / 9.5                     | 0.63 / 9.7                     | 0.68 / 9.9                           | 7.9  |
|                         |                  | 2.7   | 0.05                          | 0.56 / 9                       | 0.63 / 9.2                     | 0.67 / 9.4                           | 7.8  |
|                         |                  | 0.5   | 0.15                          | 0.7 / 9.5                      | 0.81 / 9.7                     | 0.85 / 9.9                           | 2.3  |
|                         |                  | 0.5   | 0.05                          | 0.69 / 9                       | 0.79 / 9.1                     | 0.83 / 9.4                           | 2.1  |
|                         |                  | 1.6   | 0.1                           | 0.62 / 9.3                     | 0.71 / 9.5                     | 0.75 / 9.7                           | 5.1  |
|                         |                  | 1.6   | 0.17                          | 0.63 / 9.6                     | 0.72 / 9.8                     | 0.76 / 10                            | 5.2  |
|                         |                  | 1.6   | 0.03                          | 0.61 / 8.9                     | 0.7 / 9                        | 0.75 / 9.3                           | 5    |
|                         |                  | 3.2   | 0.1                           | 0.55 / 9.3                     | 0.6 / 9.5                      | 0.64 / 9.7                           | 9    |
|                         |                  | 0.045 | 0.1                           | 0.76 / 9.3                     | 0.89 / 9.5                     | 0.92 / 9.7                           | 1.1  |
| $d_g = 4.5 \mu\text{m}$ | $v$ [mm/s] $\mu$ |       | Width/length<br>LB [mm]<br>0° | Width/length<br>LB [mm]<br>45° | Width/length<br>LB [mm]<br>90° | Depth [ $\mu\text{m}$ ] at<br>8.1 mm |      |
|                         |                  | 2.7   | 0.15                          | 0.52 / 10.2                    | 0.62 / 10.4                    | 0.66 / 10.7                          | 10.9 |
|                         |                  | 2.7   | 0.05                          | 0.51 / 9.7                     | 0.61 / 9.8                     | 0.66 / 10.1                          | 10.8 |
|                         |                  | 0.5   | 0.15                          | 0.65 / 10.2                    | 0.78 / 10.4                    | 0.82 / 10.7                          | 5.3  |
|                         |                  | 0.5   | 0.05                          | 0.64 / 9.7                     | 0.76 / 9.8                     | 0.8 / 10.1                           | 5.1  |
|                         |                  | 1.6   | 0.1                           | 0.57 / 10                      | 0.68 / 10.1                    | 0.72 / 10.4                          | 8.1  |
|                         |                  | 1.6   | 0.17                          | 0.58 / 10.3                    | 0.69 / 10.4                    | 0.73 / 10.7                          | 8.2  |
|                         |                  | 1.6   | 0.03                          | 0.56 / 9.6                     | 0.67 / 9.7                     | 0.71 / 10                            | 8    |
|                         |                  | 3.2   | 0.1                           | 0.49 / 10                      | 0.58 / 10.1                    | 0.60 / 10.4                          | 12   |
|                         |                  | 0.045 | 0.1                           | 0.73 / 10                      | 0.85 / 10.1                    | 0.89 / 10.4                          | 3.8  |

models for the above listed lids (e.g. at a distance of 6 mm from the top of the workpiece for *l* and *w* and at the distance of 8.1 mm from the top of workpiece for *d*) are presented below.

- Stochastic models for rolling direction of tinplate at  $d_g = 5.6 \mu\text{m}$ :

$$l = 8.96064 + 5.568\mu - 1.2\mu^2 - 0.124298v + 0.038843v^2,$$

$$w = 0.71475 + 0.2707\mu - 0.75\mu^2 - 0.104611v + 0.0129132v^2,$$

$$d = 1.11806 + 2.84427\mu - 3.3\mu^2 + 2.76905v - 0.4545v\mu - 0.0481405v^2.$$

- Stochastic models for a direction of 45° to rolling of tinplate at  $d_g = 5.6 \mu\text{m}$ :

$$l = 9.37555 + 4.361\mu - 1.2\mu^2 - 0.00793388v + 0.00247934v^2,$$

$$w = 0.81726 + 0.52415\mu - 1.29\mu^2 - 0.113895v - 0.09090\mu v - 0.011797v^2,$$

$$d = 1.11806 + 2.84427\mu - 3.3\mu^2 + 2.76905v - 0.4545v\mu - 0.0481405v^2$$

- Stochastic models for a direction of 90° to rolling of tinplate at  $d_g = 5.6 \mu\text{m}$ :

$$l = 9.31308 + 5.908\mu - 0.4\mu^2 - 0.00264464v - 0.000826446v^2,$$

$$w = 0.85958 + 0.38442\mu - 0.83\mu^2 - 0.11212v - 0.04545\mu v - 0.010681v^2,$$

$$d = 1.11806 + 2.84427\mu - 3.3\mu^2 + 2.76905v - 0.4545v\mu - 0.0481405v^2.$$

- Stochastic models for rolling direction of tinplate at  $d_g = 6.7 \mu\text{m}$ :

$$l = 8.65198 + 7.7145\mu - 13.7\mu^2 + 0.0244628v - 0.00764463v^2,$$

$$w = 0.73475 + 0.2707\mu - 0.75\mu^2 - 0.104611v + 0.0129132v^2,$$

$$d = 0.658439 + 3.34427\mu - 5.8\mu^2 + 2.70339v - 0.4545v\mu - 0.032644v^2.$$

- Stochastic models for a direction of 45° to rolling of tinplate at  $d_g = 6.7 \mu\text{m}$ :

$$l = 8.60072 + 11.0453\mu - 23.7\mu^2 + 0.081281v - 0.454545\mu v - 0.00764463v^2,$$

**Table 4 – Comparison of the calculated results with the measured values at 0° (6 mm from the top of workpiece for *l* and *w* 8.1 mm from the top of workpiece for *d*)**

| $d_g = 5.6 \mu\text{m}$ | Number of experiment | Calculated <i>w</i> [mm] | Measured <i>w</i> [mm] | Calculated <i>l</i> [mm] | Measured <i>l</i> [mm] | Calculated <i>d</i> [ $\mu\text{m}$ ] | Measured <i>d</i> [ $\mu\text{m}$ ] |
|-------------------------|----------------------|--------------------------|------------------------|--------------------------|------------------------|---------------------------------------|-------------------------------------|
|                         | 1.                   | 0.550168                 | 0.55                   | 9.716401                 | 9.7                    | 8.41187                               | 8.4                                 |
| 2.                      | 0.538098             | 0.54                     | 9.183601               | 9.2                      | 8.31616                | 8.3                                   |                                     |
| 3.                      | 0.689403             | 0.68                     | 9.716402               | 9.7                      | 2.80885                | 2.8                                   |                                     |
| 4.                      | 0.677333             | 0.67                     | 9.183602               | 9.2                      | 2.61315                | 2.6                                   |                                     |
| 5.-9.                   | 0.6                  | 0.60                     | 9.406001               | 9.4                      | 5.60401                | 5.6                                   |                                     |
| 10.                     | 0.604774             | 0.61                     | 9.773081               | 9.8                      | 5.68983                | 5.7                                   |                                     |
| 11.                     | 0.587876             | 0.59                     | 9.027161               | 9                        | 5.48584                | 5.5                                   |                                     |
| 12.                     | 0.531796             | 0.53                     | 9.505439               | 9.5                      | 9.59205                | 9.5                                   |                                     |
| 13.                     | 0.729639             | 0.74                     | 9.499925               | 9.5                      | 1.49195                | 1.5                                   |                                     |
| $d_g = 6.7 \mu\text{m}$ | Numb. of exp.        | Calculated <i>w</i> [mm] | Measured <i>w</i> [mm] | Calculated <i>l</i> [mm] | Measured <i>l</i> [mm] | Calculated <i>d</i> [ $\mu\text{m}$ ] | Measured <i>d</i> [ $\mu\text{m}$ ] |
|                         | 1.                   | 0.570168                 | 0.57                   | 9.511225                 | 9.5                    | 7.906685                              | 7.9                                 |
| 2.                      | 0.558098             | 0.56                     | 9.013775               | 9                        | 7.810973               | 7.8                                   |                                     |
| 3.                      | 0.709403             | 0.7                      | 9.511225               | 9.5                      | 2.339026               | 2.3                                   |                                     |
| 4.                      | 0.697333             | 0.69                     | 9.013775               | 9                        | 2.143324               | 2.1                                   |                                     |
| 5.-9.                   | 0.62                 | 0.62                     | 9.306                  | 9.3                      | 5.104001               | 5.1                                   |                                     |
| 10.                     | 0.624774             | 0.63                     | 9.587085               | 9.6                      | 5.177576               | 5.2                                   |                                     |
| 11.                     | 0.607876             | 0.61                     | 8.890655               | 8.9                      | 4.973586               | 5                                     |                                     |
| 12.                     | 0.551796             | 0.55                     | 9.28643                | 9.3                      | 9.105999               | 9                                     |                                     |
| 13.                     | 0.749639             | 0.76                     | 9.287515               | 9.3                      | 1.054407               | 1.1                                   |                                     |
| $d_g = 4.5 \mu\text{m}$ | Numb. of exp.        | Calculated <i>w</i> [mm] | Measured <i>w</i> [mm] | Calculated <i>l</i> [mm] | Measured <i>l</i> [mm] | Calculated <i>d</i> [ $\mu\text{m}$ ] | Measured <i>d</i> [ $\mu\text{m}$ ] |
|                         | 1.                   | 0.524712                 | 0.52                   | 10.21123                 | 10.2                   | 10.92222                              | 10.9                                |
| 2.                      | 0.509442             | 0.51                     | 9.713775               | 9.7                      | 10.8265                | 10.8                                  |                                     |
| 3.                      | 0.649549             | 0.65                     | 10.21123               | 10.2                     | 5.2485                 | 5.3                                   |                                     |
| 4.                      | 0.639279             | 0.64                     | 9.713775               | 9.7                      | 5.052798               | 5.1                                   |                                     |
| 5.-9.                   | 0.571996             | 0.57                     | 10.006                 | 10                       | 8.104005               | 8.1                                   |                                     |
| 10.                     | 0.585977             | 0.58                     | 10.28709               | 10.3                     | 8.214329               | 8.2                                   |                                     |
| 11.                     | 0.558599             | 0.56                     | 9.590655               | 9.6                      | 8.01034                | 8                                     |                                     |
| 12.                     | 0.519624             | 0.49                     | 9.98643                | 10                       | 12.06413               | 12                                    |                                     |
| 13.                     | 0.732475             | 0.73                     | 9.987515               | 10                       | 3.867038               | 3.8                                   |                                     |

$$w = 0.83726 + 0.52415\mu - 1.29\mu^2 - 0.11389v - 0.09090\mu v - 0.011797v^2,$$

$$d = 0.658439 + 3.34427\mu - 5.8\mu^2 + 2.70339v - 0.4545v\mu - 0.032644v^2.$$

- Stochastic models for a direction of 90° to rolling of tinplate at  $d_g = 6.7 \mu\text{m}$ :

$$l = 9.05198 + 7.7145\mu - 13.7\mu^2 + 0.0244628v - 0.00764463v^2,$$

$$w = 0.88930 + 0.19907\mu - 0.08\mu^2 - 0.11047v - 0.045454\mu v - 0.0101653v^2,$$

$$d = 0.658439 + 3.34427\mu - 5.8\mu^2 + 2.70339v - 0.4545v\mu - 0.032644v^2.$$

- Stochastic models for rolling direction of tinplate at  $d_g = 4.5 \mu\text{m}$ :

$$l = 9.35198 + 7.7145\mu - 13.7\mu^2 + 0.0244628v - 0.00764463v^2,$$

$$w = 0.69310 + 0.3367\mu + 1.08\mu^2 - 0.11386v + 0.0142975v^2,$$

$$d = 3.5373 + 1.84427\mu + 1.7\mu^2 + 2.90036v - 0.4545v\mu - 0.0791322v^2.$$

- Stochastic models for a direction of 45° to rolling of tinplate at  $d_g = 4.5 \mu\text{m}$ :

$$l = 9.58291 + 9.8945\mu - 22.1\mu^2 - 0.316694v + 0.0989669v^2,$$

$$w = 0.81331 + 0.31842\mu - 0.5\mu^2 - 0.11704v - 0.045454\mu v - 0.013429v^2,$$

$$d = 3.5373 + 1.84427\mu + 1.7\mu^2 + 2.90036v - 0.4545v\mu - 0.0791322v^2.$$

- Stochastic models for a direction of 90° to rolling of tinplate at  $d_g = 4.5 \mu\text{m}$ :

$$l = 9.78666 + 7.0545\mu - 7.9\mu^2 - 0.0138843v + 0.00433884v^2,$$

$$w = 0.85275 + 0.21615\mu - 0.25\mu^2 - 0.106308v - 0.090909\mu v - 0.010847v^2,$$

$$d = 3.5373 + 1.84427\mu + 1.7\mu^2 + 2.90036v - 0.4545v\mu - 0.0791322v^2.$$

Table 3 presents measured results for the same listed suppositions as for listed stochastic models. It is important to notice that the application of the stochastic modeling gives excellent results in comparison with experimental measured values (Table 4).

## 8. Conclusion

It is useful to perform stochastic modeling before the expensive processing procedure, before LB occurrence. In this way, savings in the process, possible improvements and final decisions can be made from the start off stage of the process. One of the most important problems in the production engineering is assurance of geometrical stability of semiproducts, which is the basis for the further successful automatic assembling (Nastran and Kuzman, 2002).

In this research the results obtained from stochastic analysis (by means of the multifactorial experimental design-rotatable design) and experimental investigations show that the results of LB modeling and finally LB appearance are very close to the experimental ones. Thus, it is possible to find out the length, width and depth of LB as a final factor in the decision of whether material should be processed or not. Also, the developed computer procedure enables a fast overview of the existing situation regarding LB behavior. Verification of the developed procedures is confirmed through rotatable experimental design.

Also, this study means defining the correlation among the parameters of this process in order to improve the existing one and to raise it to a higher techno-economic level. In this way the process parameters have become better understood. It can be concluded that the coefficient of friction, tool velocity and material properties have a different effect on LB formation and propagation in the stamping process. Also, according to stochastic modeling and the developed computer procedure, parameters that will have a significant effect on LB behavior in these processes can be concluded.

## Acknowledgements

The authors would like to acknowledge the financial support provided by the Croatian Ministry of Science, Education and Sports which enabled project Numerical Modelling, Simulation and Optimization in Sheet Metal Forming (code: 069-1201787-1754, head: Branimir Barisic, PhD.). Many thanks as well go to the company MGK-Pack (Rijeka, Croatia) which helped the study regarding materials.

## REFERENCES

Ananthan, V.S., Hall, E.O., 1987. Microscopic shear bands at Lüders fronts in mild steel. *Scripta Metall.* 21 (4), 519-520.  
 Ananthan, V.S., Hall, E.O., 1991. Macroscopic aspects of Lüders band deformation in mild steel. *Acta Metall. Mater.* 39 (12), 3153-3160.  
 Barisic, B., 2005. Lüders' bands phenomenon analysis in the process of thin-walled sheet products manufacture, faculty of engineering. Rijeka.

Barisic, B., Cukor, G., Math, M., 2004. Estimate of consumed energy at backward extrusion process by means of modelling approach. *J. Mater. Process. Technol.* 153-154 (10), 907-912.  
 Casarotto, L., Tutsch, R., Ritter, R., Weidenmüller, J., Ziegenbein, A., Klose, F., Neuhauser, H., 2003. Propagation of deformation bands investigated by laser scanning extensometry. *Comp. Mater. Sci.* 26, 210-218.  
 Čaušević, M., 1979. *Teorija plastične prerade metala*. Svjetlost, Sarajevo.  
 Conrad, H., 1962. Effect of stress on the Lüders band velocity in low carbon steels. *J. Mech. Phys. Solids* 11 (6), 437-440.  
 Corona, E., Shaw, J.A., Iadicola, M.A., 2002. Buckling of steel bars with Lüders bands. *Int. J. Solids Struct.* 39, 3313-3336.  
 Cottrell, A.H., 1948. Effect of solute atoms on the behaviour of dislocations, conference on the strength of solids. *Phys. Soc.* 16, 30-38.  
 Dhar, A., Clapham, L., Atherton, D.L., 2002. Influence of Lüders bands on magnetic Barkhausen noise and magnetic flux leakage signals. *J. Mater. Sci.* 37, 2441-2446.  
 The European Standard EN 10202: 2001, cold reduced tinmill products, electrolytic tinplate and electrolytic chromium/chromium oxide-coated steel, the European Standard Publications, Brussels, 2001.  
 Gantar, G., Kuzman, K., 2005. Optimization of stamping processes aiming at maximal process stability. *J. Mater. Process. Technol.* 167 (2-3), 237-243.  
 Gilman, J.J., 1959. Dislocations sources in crystal. *J. Appl. Phys.* 30, 1584-1594.  
 Hähner, P., 1993. Modelling of propagative plastic instabilities. *Scripta Metall. Mater.* 21 (29), 1171-1176.  
 Hartmann, L., 1896. *Distribution des deformations dans les metaux soumis aux efforts*. Paris.  
 Iricibar, R., Panizza, G., Mazza, J., 1977. On the Lüders band front in mild steel II. *Acta Metall.* 25 (10), 1169-1177.  
 Jones, H.N., Feng, C.R., 2001. Thermal activation of flow stress transients in mild steel. *Mater. Sci. Eng. A* 309-310, 92-96.  
 Kuroda, M., Yamanaka, S., Yamada, K., Isobe, Y., 2001. Evaluation of residual stresses and plastic deformations for iron-based materials by L magnetic flux sensors. *J. Alloys Compd.* 314, 232-239.  
 Lomer, W.M., 1952. The Yield phenomenon in polycrystalline mild. *J. Mech. Phys. Solids* 1 (1), 64-68.  
 Louche, H., Chrysochoos, A., 2000. An infrared image processing to analyse the calorific effects accompanying strain localisation. *Int. J. Eng. Sci.* 38, 1759-1788.  
 Low, J.R., Gensamer, M., 1944. Ageing and yield point in steel. *Trans. AIME* 158, 207-242.  
 Lüders, W., 1860. Über die äusserung der elasticität an stahlartigen eisenstäben und stahlstäben, und über eine beim biegen solcher stäbe beobachtete molecularbewegung. *Dingler's Polytech. J.* 155, 18-22.  
 Nastran, M., Kuzman, K., 2002. Stabilisation of mechanical properties of the wire by roller straightening. *J. Mater. Process. Technol.* 125-126, 711-719.  
 Nelson, B.L., 1995. *Stochastic Modelling, Analysis and Simulation*. McGraw Hill Inc., New York.  
 Pepelnjak, T., Barisic, B., 2007. Analysis and elimination of the stretcher strains on TH 415 tinplate rings in the stamping process. *J. Mater. Process. Technol.* 186 (1-3), 111-119.  
 Piobert, G., Morin, A.J., Didion, I., 1842. *Commission des principes du tir, mémorial de l'artillerie* 5, 501-552.  
 Rowcliffe, A.F., Zinkle, S.J., Hoelzer, D.T., 2000. Effect of strain rate on the tensile properties of unirradiated and irradiated V-4Cr-4Ti. *J. Nucl. Mater.* 283-287, 508-512.

- Sun, H.B., Yoshida, F., Ma, X., Kamei, T., Ohmori, M., 2000. Finite element simulation on the propagation of Lüders band and effect of stress concentration. *Mater. Sci. Eng. A* 250, 300–308.
- Sylwestrowicz, W., Hall, E.O., 1951. The deformation and ageing of mild steel. *Proc. Phys. Soc. B* 64, 495–502.
- Tay, F.E.H., Sikdar, S.K., Mannan, M.A., 2002. Topography of the flank wear surface. *J. Mater. Process. Technol.* 120 (1–3), 243–248.
- Thomas, T.Y., 1954. A discussion of the load drop and related matters associated with the formation of Lüders band. *Proc. Natl. Acad. Sci.* 40, 572–576.
- Thomas, T.Y., 1958. The Lüders band problem. *J. Math. Mech.* 2 (7), 141–148.
- Tsukahara, H., Iung, T., 1998. Finite element simulation of the Piobert-Lüders behavior in an uniaxial tensile test. *Mater. Sci. Eng. A* 248, 304–308.
- Wattrisse, B., Chrysochoos, A., Muracciole, J.M., Gaillard, M.N., 2001. Kinematic manifestations of localisation phenomena in steels by digital image correlation. *Eur. J. Mech. A: Solids* 20, 189–211.
- Wen, W., Morris, J.G., 2004. The effect of cold rolling and annealing on the serrated yielding phenomenon of AA5182 aluminum alloy. *Mater. Sci. Eng. A* 373,204–216.